DOI: 10.1021/ma9027307

Macromolecules
ARTICLE

Ionic Liquid Distribution in Ordered Block Copolymer Solutions

Justin M. Virgili,[†,‡] Alisyn J. Nedoma,[†] Rachel A. Segalman,[†,‡] and Nitash P. Balsara*[,†,‡,§]

[†]*Department of Chemical Engineering, University of California, Berkeley, California 94720,*
[‡]*Materials Science Division, and* [§]*Energy and Environmental Technologies Division, Lawrence Berkeley National Laboratory, Berkeley, California 94720*

Received December 10, 2009; Revised Manuscript Received March 3, 2010

ABSTRACT: The distribution of an ionic liquid within microphase-separated domains of a block copolymer in mixtures of the two components is studied using contrast-matched small-angle neutron scattering (SANS) and differential scanning calorimetry (DSC). In concentrated mixtures of a poly(styrene-*block*-2-vinyl pyridine) (S2VP) copolymer in an imidazolium bis(trifluoromethane)sulfonimide ([Im][TFSI]) ionic liquid (block copolymer volume fraction ranging from 0.51 to 0.86), the ionic liquid preferentially pervades the poly(2-vinyl pyridine) (P2VP) blocks. Unexpected differences in the degree of partitioning into P2VP-rich and polystyrene-rich (PS) microphases are observed in mixtures with hydrogenated versus deuterated [Im][TFSI]. In the case of mixtures with hydrogenated [Im][TFSI], the microphase partition coefficient, defined as the ratio of the ionic liquid volume fraction in the PS-rich microphase relative to that in the P2VP-rich microphase, ranges from 0.0 to 0.1. In contrast, the microphase partition coefficient in mixtures with deuterated [Im][TFSI] range from 0.0 to 0.7.

Introduction

Block copolymers are an extensively studied class of materials that self-assemble on the 10 nm length scale.[1] Additives such as molecular solvents, salts, and nanoparticles have been combined with block copolymers to provide functionality, and the resulting multiphase systems are themselves topics of vibrant research. Polymer/ionic liquid mixtures have been the subject of an increasing number of publications[2] because of the opportunities created by the combination of a solid polymer support and the attractive physiochemical properties of ionic liquids, such as nonflammability, negligible vapor pressure, high ionic conductivity, and wide electrochemical stability window,[3] for applications including battery electrolytes,[4] fuel cells,[5] and field-effect transistors.[6] Block-copolymer-based electrolytes show promise in decoupling mechanical and ion-conducting properties critical for such applications.[7,8]

To date, studies of block copolymer/ionic liquid mixtures have largely explored the self-assembly of these systems from the perspective of polymer/solvent interactions over a broad range of compositions,[9−11] and these prior studies are comprehensively reviewed in ref 11. In most cases, the block copolymers contain a polar block that is miscible with the ionic liquid and a nonpolar block that is immiscible with the ionic liquid. The miscible block forms the functional ion-transporting channel, whereas the immiscible block provides mechanical stability. To our knowledge, there are no prior studies of the distribution of an ionic liquid within block copolymer microphases. This knowledge is crucial for enabling applications because high concentrations of the ionic liquid in the nonpolar microphases may decrease the efficiency of ion transport and plasticize the microphases that are intended to provide mechanical stability.

Small-angle neutron scattering (SANS),[12] resonant soft X-ray scattering (RSoXS),[13] and energy-filtered transmission electron microscopy (EFTEM)[14] are techniques that can, in principle, be used to determine the distribution of a component of interest in complex, multicomponent systems. In this study, we report on the use of contrast-matched SANS to characterize the distribution of an imidazolium bis(trifluoromethane)sulfonimide ([Im][TFSI]) ionic liquid within poly(styrene-*block*-2-vinyl pyridine) (S2VP) copolymer domains (Figure 1). A simple model is presented for determining the distribution of [Im][TFSI] in PS- and P2VP-rich microphases at varying block copolymer concentrations. Together with thermal characterization of the S2VP/[Im][TFSI] mixtures using differential scanning calorimetry (DSC), we find an unexpected dependence of the partitioning of [Im][TFSI] within block copolymer domains on deuterium labeling of the ionic liquid.

Experimental Section

Polymer Synthesis and Characterization. Three S2VP copolymers were synthesized via anionic polymerization using standard methods.[15] The number-average molecular weight (M_n) of the polystyrene (PS) hompolymers and polydispersity (PDI) of each block copolymer were determined using gel permeation chromatography (GPC), and the total number-averaged molecular weights of the block copolymers were determined via ^{1}H NMR (Bruker AVB-300). The S2VP copolymers are designated as *h*S2VP(*xx*-*yy*) or *d*S2VP(*xx*-*yy*), where *xx* and *yy* refer to the number-average molecular weights in kilograms per mole of the PS and P2VP blocks, respectively, and the prefix *h* or *d* indicates a hydrogenated or deuterated PS block. For *d*S2VP, d_8-styrene monomer (Polymer Source) was utilized. In Table 1, the M_n, PS volume fraction (f_{PS}), and polydispersities of all copolymers are given.

Ionic Liquid Purification. Imidazole (≥95%) and bis(trifluoromethane)sulfonimide (HTFSI, ≥95%) were purchased from Sigma Aldrich and *d*-imidazole (d_4, ≥98% deuteration, ≥98% purity) was purchased from Cambridge Isotopes. Each compound was purified by sublimation under vacuum. DSC was used to assess the purity of the starting materials. Purified imidazole and HTFSI were combined in equimolar quantities in a glovebox, sealed, and heated in an oven outside the glovebox to 100 °C for 2 to 3 h to prepare the ionic liquid [Im][TFSI].

*Corresponding author. E-mail: nbalsara@berkeley.edu.

 Published on Web 03/29/2010

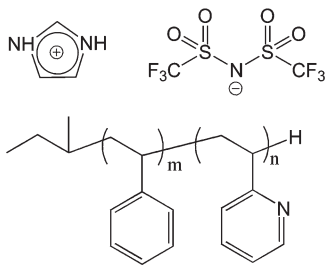

Figure 1. Chemical structure of imidazole and HTFSI ions and poly(styrene-*block*-2-vinyl pyridine) copolymer.

Table 1. Characteristics of Copolymers Used in this Study

block copolymer	M_n PS (g/mol)	M_n P2VP (g/mol)	f_{PS}	PDI
*d*S2VP(7-7)	7100	6800	0.50	1.10
*h*S2VP(7-7)	7400	7000	0.48	1.13
*h*S2VP(12-12)	12 000	12 400	0.49	1.19

The composition of both [*h*Im][TFSI] and [*d*Im][TFSI], where the prefix *h* or *d* indicates a hydrogenated or deuterated imidazolium cation, respectively, was confirmed by comparing the melting point (72−74 °C) with literature.[16]

Small-Angle Neutron Scattering Sample Preparation and Methods. Dichloromethane was degassed using three freeze, pump, thaw cycles, stirred over CaH_2 overnight, then distilled into a collection flask, brought into a glovebox, and stored on molecular sieves. Predetermined quantities of [*h*Im][TFSI], [*d*Im][TFSI], *h*S2VP(7-7), *h*S2VP(12-12), and *d*S2VP(7-7) were weighed in glass vials, and ca. 5 wt % solutions were prepared using dichloromethane in the glovebox. Solutions were stirred overnight. Samples were cast into sample cells with an aluminum spacer sealed onto a quartz window on one side in the glovebox. The polymer/ionic liquid solution was put in the sample cell one drop at a time. Solvent was allowed to evaporate before the addition of the next drop until a ca. 1 mm solid sample was obtained in the sample cell. Samples were heated to 60 °C (above the boiling point of dichloromethane) in the glovebox for ca. 18 h to remove remaining solvent and then annealed 2 to 3 h at 145 °C inside the glovebox. A second quartz window was glued to seal the samples in the glovebox, which were stored with desiccant when outside the glovebox to reduce the chance of water contamination. Samples are designated by the value of the estimated polymer volume fraction, ϕ_P, assuming ideal mixing. The densities of [*h*Im][TFSI] and [*d*Im][TFSI] were estimated to be 1.67 and 1.69 g/cm^3, respectively, from scattering length density fits of SANS intensity profiles presented in this article. The densities of *h*PS, *d*PS, and P2VP were taken to be 1.05, 1.12, and 1.05 g/cm^3, respectively.[17,18]

SANS measurements were performed at the National Institute of Standards and Technology (NIST) on the NG7 SANS instrument.[19] Neutrons with a 6 Å wavelength and a sample-to-detector distance of 13, 4.5, and 1 m were utilized at NIST. Data from room-temperature samples were collected, and the intensity was corrected for instrumental background, empty cell scattering, sample transmission, and incoherent background with user-facility developed software.[20] This gives the coherent scattering intensity, I, as a function of the magnitude of the scattering vector, q, $q = (4\pi/\lambda)\sin(\theta/2)$, where λ is the neutron wavelength and θ is the scattering angle. In some samples, a small positive scattering intensity in the range of 0.1 cm^{-1} remained after this data reduction procedure probably due to the fact that our procedures for correcting for incoherent scattering are approximate.[12] In these cases, the residual intensity was removed by subtracting the average intensity over the range $0.40 < q < 0.59$ Å^{-1}.

Differential Scanning Calorimetry Sample Preparation and Methods. DSC was performed on a TA Instruments DSC 2920. Samples were solution cast in a glovebox into aluminum DSC pans from the same solutions used to prepare scattering samples. The samples were heated to 60 °C in the glovebox for ca. 18 h to remove remaining solvent and then annealed 2 to 3 h at 145 °C inside the glovebox. The samples were then crimped within the glovebox using hermetically sealed pans and placed inside a container with desiccant for transfer to the DSC. Indium and dodecane were used as calibration standards for the DSC. Samples underwent three heating and cooling cycles to ensure reproducibility.

Results and Discussion

Experimental Observations. Representative SANS profiles from mixtures with a fixed polymer concentration $\phi_P = 0.86$ are shown in Figure 2. All scattering profiles were recorded at 30 °C. The parameter f_d, defined as the volume fraction of *d*S2VP(7-7) in the mixture without ionic liquid, indicates the composition of the deuterated polymer in each mixture. S2VP/[*h*Im][TFSI] data are shown in Figure 2a. The mixture with $f_d = 1.00$ exhibits a lamellar morphology with peaks at $q = q^*$, $2q^*$, and $3q^*$ (where q^* is the magnitude of the scattering vector at the primary peak). The introduction of *h*S2VP(7-7), that is, decreasing f_d, results in a decrease in the intensity of the primary peak and a loss of higher order peaks due to a decrease in the neutron scattering contrast between the PS-rich and the P2VP-rich lamellae. At $f_d = 0.20$, the primary peak is absent, indicating a perfect match in the contrasts of the PS-rich and the P2VP-rich lamellae. Further reduction of f_d leads to an increase in scattering intensity of the primary peak. At $f_d = 0.10$, higher order peaks corresponding to the lamellar phase reappear. Qualitatively similar results are obtained from S2VP/[*d*Im][TFSI] mixtures with the contrast matching condition occurring at $f_d = 0.25$, as shown in Figure 2b. The center-to-center distance between adjacent PS lamellae, $l = 2\pi/q^*$, is 19.8 ± 0.2 nm in the $f_d = 1.00$ samples in both [*h*Im][TFSI] and [*d*Im][TFSI] ionic liquids, indicating that deuteration of imidazole does not influence the observed morphology. The small change in l observed in both [*h*Im][TFSI] and [*d*Im][TFSI] mixtures with S2VP copolymer as f_d is varied and is probably caused by a slight mismatch of molecular weight in the *h*S2VP(7-7) and *d*S2VP(7-7) copolymers. Additional contrast matching experiments were performed on $\phi_P = 0.70$ and 0.51 S2VP copolymer mixtures in both [*h*Im][TFSI] and [*d*Im][TFSI]. The SANS profiles of these samples are shown in Figures S1 and S4 in the Supporting Information.

SANS Contrast Matching Methodology. The scattering intensity from a given sample wherein only f_d is varied is given by ref 21

$$I(q^*) \propto (b_{S,\mathrm{eff}} - b_{V,\mathrm{eff}})^2 \quad (1)$$

where $I(q^*)$ is the primary peak scattering intensity and $b_{i,\mathrm{eff}}$ is the effective scattering length density of microphase i (S implies PS-rich microphase and V implies P2VP-rich microphase). Assuming a homogeneous distribution of [Im][TFSI] within PS-rich and P2VP-rich microphases, we can write $b_{i,\mathrm{eff}}$ as

$$b_{i,\mathrm{eff}} = \sum_j \phi_{i,j} b_j \quad (2)$$

where $\phi_{i,j}$ is the mean intrablock volume fraction of component j (j = PS, P2VP, or IL) within microphase i and b_j is the scattering length density of component j, given in Table 2. Therefore, as an example, the intrablock volume fraction of ionic liquid within the PS-rich microphase is given by $\phi_{S,IL}$.

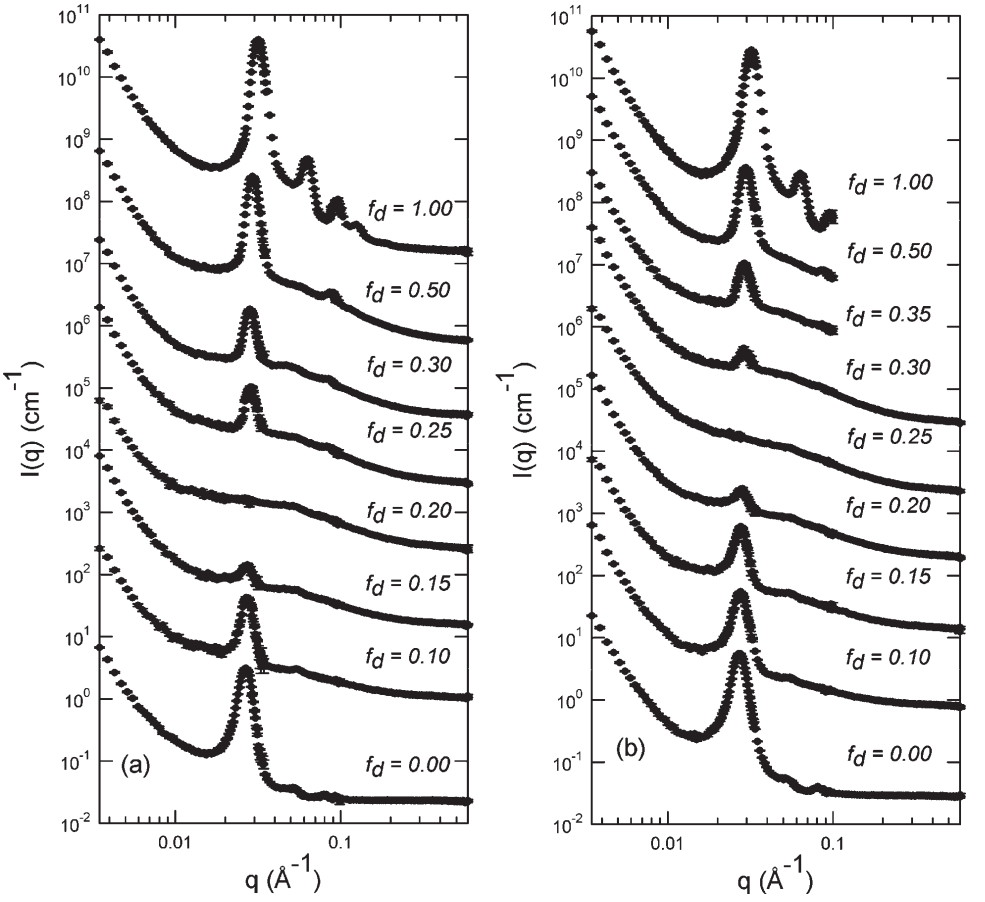

Figure 2. SANS intensity profiles (offset for clarity) as a function of scattering vector q for $\phi_P = 0.86$ mixtures in (a) [*h*Im][TFSI] and (b) [*d*Im][TFSI] with varying f_d of the *h*S2VP(7-7)/*d*S2VP(7-7) copolymers at 30 °C. In all cases, the individual intensity profiles are labeled with the volume fraction of *d*S2VP.

Table 2. Scattering Length Densities of Polymers and Ionic Liquids

component	neutron, b/v × 10^6 (Å^{-2})	volume (Å^3)
*h*PS	1.41	179
*d*PS	6.40	179
P2VP	1.96	179
[*h*Im][TFSI]	3.06	347
[*d*Im][TFSI]	5.04	347

A full list of variable definitions is available in Table S1 in the Supporting Information. The intrablock volume fractions, $\phi_{i,j}$, of each microphase i is constrained by

$$\sum_j \phi_{i,j} = 1 \tag{3}$$

We introduce a variable, f_S, the volume fraction of the PS-rich microphase swollen with ionic liquid. By definition, f_V, the volume fraction of the P2VP microphase swollen with ionic liquid, is given by

$$f_V = 1 - f_S \tag{4}$$

The intrablock volume fractions of ionic liquid within the microphases, $\phi_{S,IL}$ and $\phi_{V,IL}$, are related by the following ionic liquid material balance

$$\phi_{V,IL} = \left(\frac{(1-\phi_P) - f_S \times \phi_{S,IL}}{f_V} \right) \tag{5}$$

The degrees of mixing between the PS/P2VP blocks, quantified by $\phi_{S,P2VP}$ and $\phi_{V,PS}$, are related by the following PS material balance

$$\phi_{V,PS} = \left(\frac{f_{PS} \times \phi_P - f_S \times \phi_{S,PS}}{f_V} \right) \tag{6}$$

where f_{PS} is the known volume fraction of PS in the neat copolymer and ϕ_P is the known overall volume fraction of polymer in the mixtures. Equations 2−6 contain eight unknown variables, and thus there are three independent variables that we determine from the SANS data: $\phi_{S,IL}$, $\phi_{S,P2VP}$, and f_S. Previous studies that have examined the effect of deuteration on polymer thermodynamics suggest that the effect of deuterium labeling of PS chains on thermodynamics should be negligible.[22−25] We thus assume that changes in f_d do not affect the distribution of the components.

Primary peak intensities, $I(q^*)$, were extracted from the SANS data assuming a power law background in the vicinity of the peak. We focus on $I(q^*)/I_h(q^*)$, which is the peak intensity normalized by the peak intensity of the $f_d = 0.00$ sample. We determined initial values of f_S and f_V for calculating $I(q^*)/I_h(q^*)$ by assuming that all of the ionic liquid pervades the P2VP-rich microphase ($\phi_{S,IL} = 0.00$) using a material balance on P2VP and ionic liquid in the P2VP-rich microphase (eq 7). An iterative procedure based on eq 7 was used to recalculate the values of f_S and f_V as the

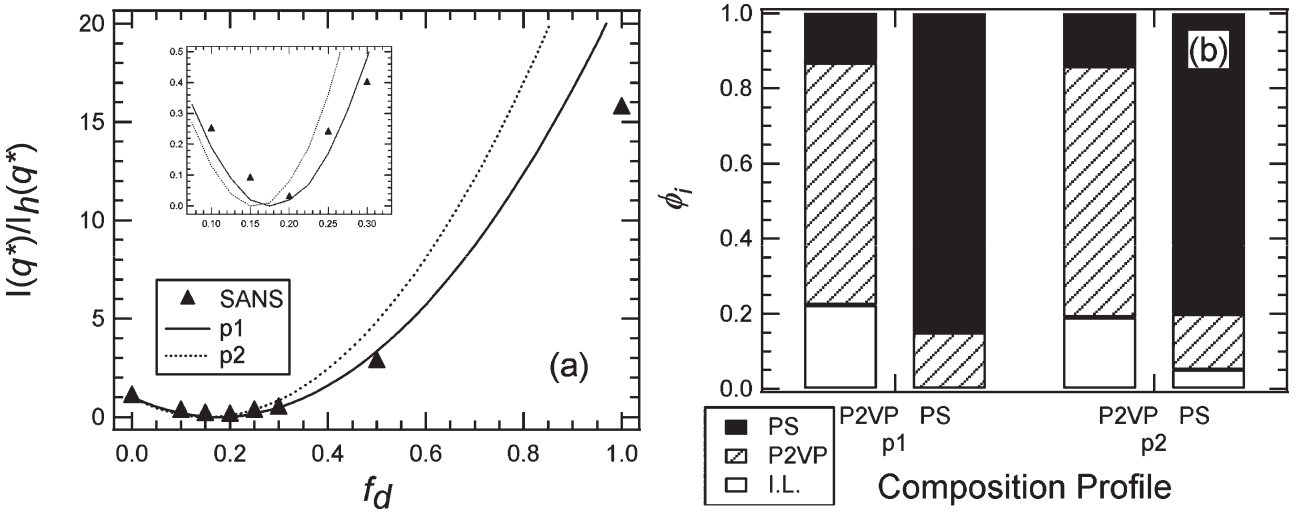

Figure 3. (a) Comparison of experimentally measured and modeled $I(q^*)/I_h(q^*)$ for $\phi_P = 0.86$ solutions in [*h*Im][TFSI] as a function of f_d at 30 °C. Inset shows detail near contrast match composition. (b) Composition of PS-rich and P2VP-rich microphases in $\phi_P = 0.86$ S2VP copolymer/[*h*Im][TFSI] mixtures for profiles *p*1 and *p*2 corresponding to $I(q^*)/I_h(q^*)$ profiles in part a.

partitioning of ionic liquid and mixing between PS/P2VP blocks was varied

$$f_V = f_{P2VP}\phi_P + (1-\phi_P)\left(\frac{f_V^\dagger \times \phi_{V,IL}^\dagger}{f_V^\dagger \times \phi_{V,IL}^\dagger + f_S^\dagger \times \phi_{S,IL}^\dagger}\right) \quad (7)$$

where a † superscript denotes the corresponding composition values for the prior iteration and f_{P2VP} is the known volume fraction of P2VP in the neat copolymer. The iterations were repeated until the calculated and measured dependence of $I(q^*)/I_h(q^*)$ on f_d were in agreement.

From our previous work, we have found that S2VP/[Im][TFSI] mixtures with similar molecular weights as the copolymers used in this study exhibit strong segregation limit molecular-weight-dependent scaling behavior over a broad range of ϕ_P.[26] Helfand and Tagami have shown using self-consistent field theory (SCFT) that the interfacial width, *w*, between block copolymer domains scales as $w \approx \chi^{-1/2}$ for small values of χ,[27] where χ is the Flory−Huggins interaction parameter. Subsequently, Shull determined the dependence of *w* on χN for finite values of χN in block copolymers, where *N* is defined as the degree of polymerization.[28] In the case of block copolymers dissolved in a selective molecular solvent, Huang and Hsueh determined using SCFT that the chain intermixing increases with dilution.[29] On the basis of ref 29, we estimate that the width of the interface increases by about a factor of two or less relative to the dry state, when $\phi_P = 0.51$ (the lower limit of our experimental window). Using the argument that $\phi_{V,PS}$ and $\phi_{S,P2VP}$ are of order w/l, we obtain the restriction that $0 \le \phi_{V,PS} \le 0.15$ and $0 \le \phi_{S,P2VP} \le 0.15$. We use this restriction to evaluate the partitioning of the ionic liquid between the PS-rich and the P2VP-rich microphases.

Determination of Ionic Liquid Distribution. In Figure 3a, we compare the experimentally observed $I(q^*)/I_h(q^*)$ values (symbols) from $\phi_P = 0.86$ S2VP/[*h*Im][TFSI] with calculations (curves) based on eqs 1−7. The two curves in Figure 3a correspond to two different compositions that are labeled *p*1 and *p*2. The volume fractions of the components within the PS- and PVP-rich microphases, corresponding to profiles *p*1 and *p*2, are given in Figure 3b. Profile *p*1 assumes complete partitioning of [*h*Im][TFSI] into P2VP blocks with moderate mixing of PS and P2VP microphases ($\phi_{S,P2VP} = 0.15$, $\phi_{V,PS} = 0.13$). The predicted dependence of $I(q^*)/I_h(q^*)$ on f_d based on *p*1 exhibits a contrast match at $f_d = 0.18$ in agreement with experiments. In addition, the measured increase in $I(q^*)/I_h(q^*)$ as f_d deviates from the contrast matching point is in agreement with the predictions based on *p*1. Profile *p*2 results from the same degree of PS and P2VP mixing as *p*1, but some of the [*h*Im][TFSI] is allowed to pervade PS microphases ($\phi_{S,IL} = 0.05$ and $\phi_{V,IL} = 0.19$). The predicted dependence of $I(q^*)/I_h(q^*)$ on f_d based on *p*2 exhibits a contrast match at $f_d = 0.16$, which is well-removed from the experimental observation. In addition, profile *p*2 substantially overpredicts $I(q^*)/I_h(q^*)$ at high values of f_d.

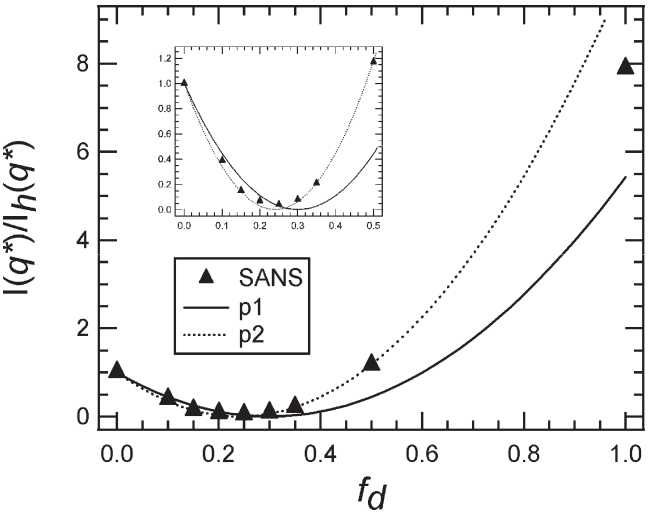

Figure 4. Comparison of experimentally measured and modeled $I(q^*)/I_h(q^*)$ for $\phi_P = 0.86$ solutions in [*d*Im][TFSI] as a function of f_d at 30 °C. Inset shows detail near contrast match composition. See Figure 3b for the composition of PS-rich and P2VP-rich microphases in $\phi_P = 0.86$ S2VP copolymer/[*d*Im][TFSI] mixtures of profiles *p*1 and *p*2.

We define a microphase partition coefficient of the ionic liquid, γ_{IL}, as

$$\gamma_{IL} = \frac{\phi_{S,IL}}{\phi_{V,IL}} \quad (8)$$

The values of γ_{IL} were determined from the best fit of the dependence of $I(q^*)/I_h(q^*)$ on f_d. Error bars for γ_{IL} are determined from the 95% confidence interval of the best fit determined from analysis of the residuals and represent a

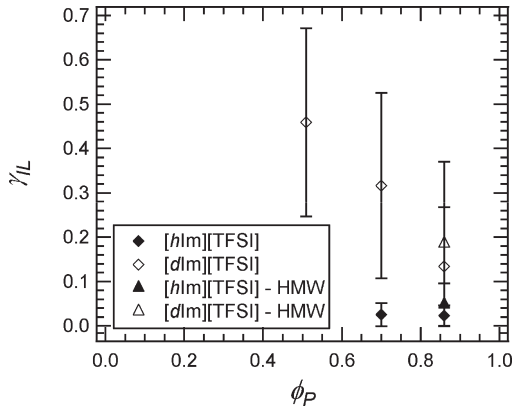

Figure 5. Ionic liquid partition coefficient (γ_{IL}) for varying S2VP/[*h*Im][TFSI] and S2VP/[*d*Im][TFSI] mixture compositions at 30 °C. For $\phi_P = 0.86$ mixtures only, "HMW" denotes the use of *h*S2VP(12-12) in place of *h*S2VP(7-7). Error bars for γ_{IL} are determined from the 95% confidence interval of the best fit determined from analysis of the residuals and represent a range of γ_{IL} values that satisfy the residuals constraint.

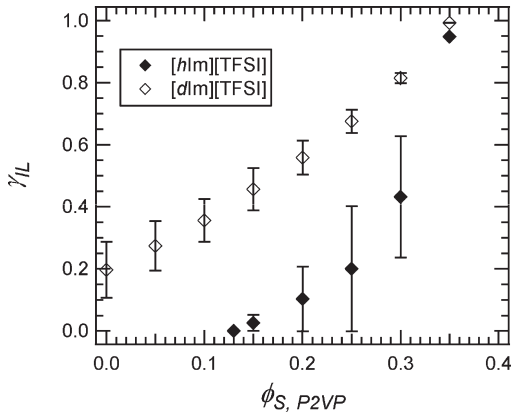

Figure 6. Ionic liquid partition coefficient (γ_{IL}) for $\phi_P = 0.70$ S2VP/[*h*Im][TFSI] and S2VP/[*d*Im][TFSI] mixtures as a function of PS/P2VP mixing ($\phi_{S,P2VP}$) at 30 °C. Error bars for γ_{IL} are determined from the 95% confidence interval of the best fit determined from analysis of the residuals and represent a range of γ_{IL} values that satisfy the residuals constraint.

range of γ_{IL} values that satisfy the residuals constraint and not a standard deviation. Using this approach, we obtain γ_{IL} for [*h*Im][TFSI] in S2VP at $\phi_P = 0.86$ to be 0.02 ± 0.02.

In Figure 4, we compare the experimentally observed $I(q^*)/I_h(q^*)$ values (symbols) from $\phi_P = 0.86$ S2VP/[*d*Im]-[TFSI] with calculations (curves) based on eqs 1−7. The two curves in Figure 4 correspond to compositions *p*1 and *p*2 defined in Figure 3b. In this case, profile *p*1, predicts a minimum at $f_d = 0.30$, which is well-removed from the experimentally observed contrast matching point. In addition, the calculated *p*1 profile severely underpredicts the value of $I(q^*)/I_h(q^*)$ at large values of f_d. In contrast, both the location of the minimum in $I(q^*)/I_h(q^*)$, and the increase in $I(q^*)/I_h(q^*)$ as the composition departs from the contrast matching point is captured by predictions based on profile *p*2. It is evident that there is a relatively large concentration of [*d*Im][TFSI] in the PS-rich microphase. On the basis of the method described above, we determine γ_{IL} for [*d*Im][TFSI] in S2VP at $\phi_P = 0.86$ to be 0.13 ± 0.13.

We repeated the analysis described above for varying ϕ_P values. Results obtained at $\phi_P = 0.70$ and $\phi_P = 0.51$ S2VP/[*h*Im][TFSI] and S2VP/[*d*Im][TFSI] mixtures are given in the Supporting Information. The results of this analysis are summarized in Figure 5, where we plot γ_{IL} versus ϕ_P for the S2VP/[*h*Im][TFSI] and S2VP/[*d*Im][TFSI] mixtures. Included in Figure 5 are additional data obtained from mixtures of *h*S2VP(12-12) and *d*S2VP(7-7) copolymers. (Our discussion thus far has been focused on mixtures of *h*S2VP(7-7) and *d*S2VP(7-7) copolymers.) The analysis indicates that γ_{IL} for [*d*Im][TFSI] ranges from 0 to 0.67, whereas that of [*h*Im][TFSI] is in the vicinity of 0 to 0.10. Despite the large error bars, it is evident that γ_{IL} increases with increasing ionic liquid concentration in the case of [*d*Im][TFSI]. The observed [*d*Im][TFSI] partitioning is not significantly affected by morphological changes; both the $\phi_P = 0.86$ and $\phi_P = 0.70$ mixtures exhibit a lamellar morphology, whereas the $\phi_P = 0.51$ mixture exhibits a hexagonally close-packed cylinder morphology.

The striking difference in partitioning of the deuterated and protonated ionic liquid in the PS- and P2VP-rich microphases, seen in Figures 3−5, is unexpected. The error bars in Figure 5 mainly reflect our inability to ascertain the extent of intermixing of the PS and P2VP chains and the fact that the calculations are constrained by $0 \le \phi_{S,P2VP} \le 0.15$ and $0 \le \phi_{V,PS} \le 0.15$. Figure 6 is a plot of γ_{IL} as a function of $\phi_{S,P2VP}$ for $\phi_P = 0.70$ S2VP mixtures in [*h*Im][TFSI] and [*d*Im][TFSI], where there are no constraints on $\phi_{S,P2VP}$ and $\phi_{V,PS}$. For the $\phi_P = 0.70$ S2VP/[*h*Im][TFSI] mixtures, a minimum degree of PS/P2VP mixing ($\phi_{S,P2VP} = 0.13$) is necessary to achieve an acceptable fit to the contrast match SANS data. As $\phi_{S,P2VP}$ is increased above this value, a range of γ_{IL} values are consistent with the SANS data as indicated in Figure 6. In the case of the S2VP/[*d*Im][TFSI] mixtures a satisfactory fit can be achieved with no PS/P2VP mixing ($\phi_{S,P2VP} = 0.00$). We thus show γ_{IL} obtained over the entire range $0 \le \phi_{S,P2VP} \le 0.35$. At $\phi_{S,P2VP}$ values above 0.35, the predictions and measured dependencies of $I(q^*)/I_h(q^*)$ on f_d are not in agreement, and the absolute upper bound for $\phi_{PS,P2VP}$ is thus 0.35. In Figure 6, we see that γ_{IL} from [*d*Im]-[TFSI] samples is significantly larger than that of [*h*Im]-[TFSI] for all values of $\phi_{S,P2VP}$. The larger value of γ_{IL} of [*d*Im][TFSI] samples is expected to lead to more intermixing, that is, a larger value of $\phi_{S,P2VP}$. This will only increase the disparity between γ_{IL} from the [*d*Im][TFSI] mixture relative to the [*h*Im][TFSI] mixture. Our conclusion that γ_{IL} is greater in the case of the deuterated ionic liquid is thus robust.

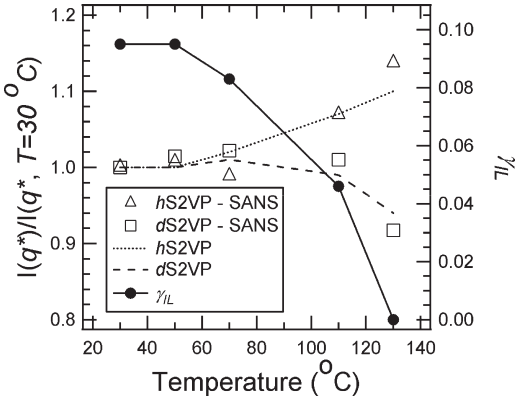

Figure 7. SANS-determined values of $I(q^*)/I(q^*, T = 30\ °C)$ of $\phi_P = 0.86$ samples with [*h*Im][TFSI] in *h*S2VP(12-12) (△) and *d*S2VP(7-7) (□) copolymers along with predicted temperature-dependent values of $I(q^*)/I(q^*, T = 30\ °C)$ (lines, left-hand axis) and γ_{IL} (−●−, right-hand axis).

In the case of the $\phi_P = 0.51$ S2VP/[*h*Im][TFSI] mixtures, we were unable to achieve a satisfactory fit to the contrast

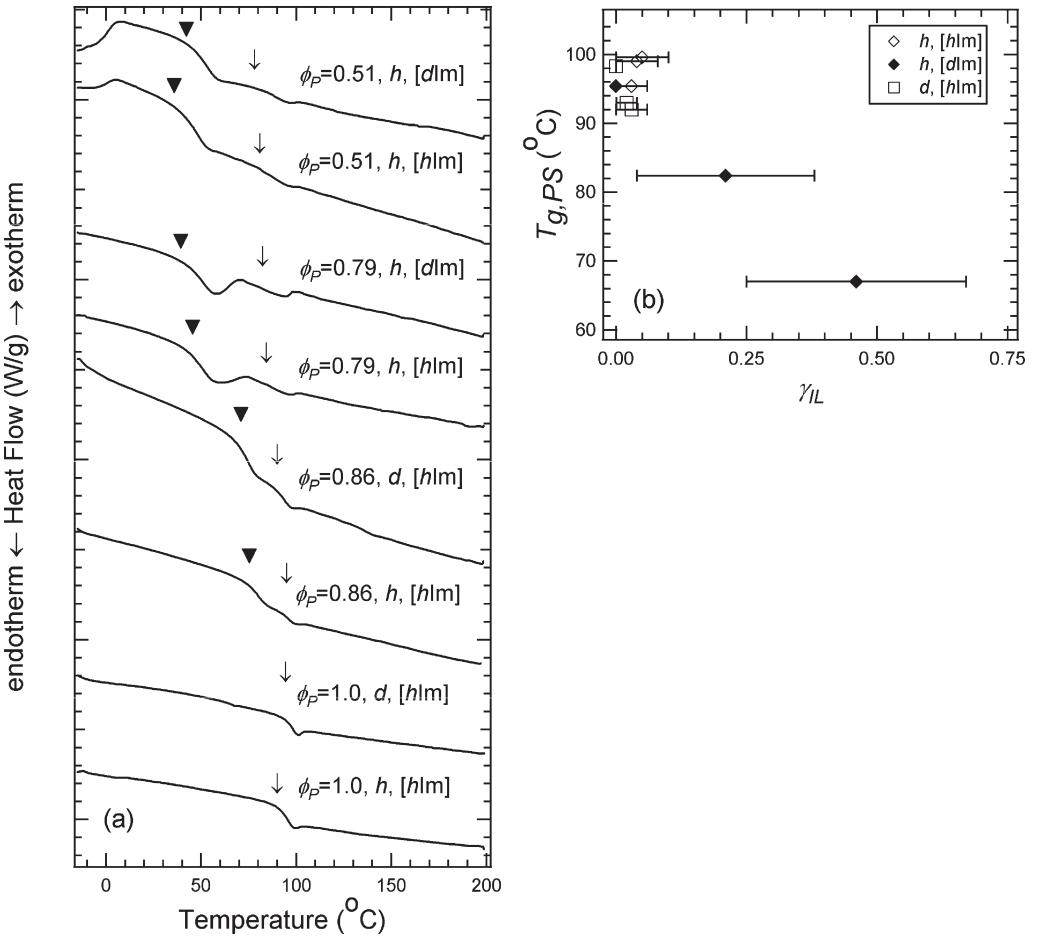

Figure 8. (a) DSC thermograms (offset for clarity) and (b) $T_{g,PS}$ versus γ_{IL} for varying S2VP/[Im][TFSI] mixture compositions and deuterium labelings. In part a, ϕ_P and high (↓) and low (▼) temperature T_g values are specified, and the heating rate is 10 °C/min. In parts a and b, *h* and *d* correspond to *h*S2VP(12-12) and *d*S2VP(7-7), respectively, whereas [*h*Im] and [*d*Im] correspond to [*h*Im][TFSI] and [*d*Im][TFSI], respectively. In part b, error bars for γ_{IL} are determined from the 95% confidence interval of the best fit determined from analysis of the residuals and represent a range of γ_{IL} values that satisfy the residuals constraint.

match SANS data with the PS/P2VP mixing constraint $\phi_{S,P2VP} \leq 0.15$. Upon relaxing the PS/P2VP mixing constraint to $\phi_{S,P2VP} \leq 0.25$, a satisfactory fit to SANS data is achieved with $\gamma_{IL} = 0.10 \pm 0.10$, a value that is similar to that found at other values of ϕ_P for the [*h*Im][TFSI] mixtures. We have not included this data point in Figure 5 because it was obtained using a different constraint on $\phi_{S,P2VP}$.

Another constraint on the value of $\phi_{S,P2VP}$ is obtained when we examine the temperature dependence of the SANS results. In Figure 7, we plot the temperature dependence of $I(q^*)/I(q^*, T = 30\ °C)$ for the $\phi_P = 0.86$ *h*S2VP(12-12)/[*h*Im]-[TFSI] and *d*S2VP(7-7)/[*h*Im][TFSI] mixtures (left-hand *y* axis). $I(q^*)/I(q^*, T = 30\ °C)$ is defined as the ratio of the SANS-determined (or calculated) $I(q^*)$ to the $I(q^*)$ of the same sample (or calculation) obtained at 30 °C. The corresponding SANS profiles are given in the Supporting Information (Figure S10). We anticipate that as the temperature of the mixture increases, the selectivity of [Im][TFSI] for the P2VP phase will decrease along with an increase in the degree of mixing between PS and P2VP blocks.[30] On the basis of the scattering length densities of the components (Table 2) and eqs 1−7, this expectation would lead to a monotonic decrease in the value of $I(q^*)/I(q^*, T = 30\ °C)$ with increasing temperature for both *h*S2VP(12-12)/[*h*Im][TFSI] and *d*S2VP-(7-7)/[*h*Im][TFSI] mixtures with increasing temperature. Instead, we observe that $I(q^*)/I(q^*, T = 30\ °C)$ of *h*S2VP-(12-12)/[*h*Im][TFSI] increases with increasing temperature. This trend can only be explained by a decrease in the partitioning of [*h*Im][TFSI] into PS microphases accompanied by an increase in PS/P2VP mixing. The contrast matching results from the $\phi_P = 0.86$ S2VP/[*h*Im][TFSI] mixtures at 30 °C indicated that $\gamma_{IL} = 0.048 \pm 0.048$ (Figure 5). Predictions of $I(q^*)/I(q^*, T = 30\ °C)$ based on eqs 1−7 are represented by the curves in Figure 7, and the right-hand *y* axis in Figure 7 shows the temperature dependence of γ_{IL} that was used in the predictions. The value of γ_{IL} at 30 °C used in these predictions is 0.095, which is at the upper end of the range of γ_{IL} established by the SANS contrast matching experiments. The temperature dependence of intermixing of the PS and P2VP blocks obtained from this analysis is given in the Supporting Information (Figure S11). Using γ_{IL} values < 0.046 at 30 °C lead to predictions that are inconsistent with experimental data. The temperature-dependent data shown in Figure 7 provide valuable additional constraints on the determination of the ionic liquid distribution within the PS and P2VP microphases.

DSC thermograms for varying ϕ_P of S2VP/[Im][TFSI] mixtures in which either PS or [Im][TFSI] is deuterated are presented in Figure 8a. For the neat copolymer samples, the T_g values of *h*S2VP(12-12) and of *d*S2VP(7-7) are 95 and 98 °C, respectively, because of the similarities of the T_g values of the PS and P2VP homopolymers. Samples with [Im][TFSI] exhibit two T_g values, the low-temperature T_g representing

the P2VP-rich microphase plasticized by [Im][TFSI] and the high-temperature T_g representing the PS-rich microphase ($T_{g,PS}$) that contains a much lower concentration of [Im][TFSI]. In Figure 8b, we plot $T_{g,PS}$ as a function of [Im][TFSI] partitioning in the PS-rich microphase determined by SANS. Error bars in Figure 8b correspond to the range of γ_{IL} values shown in Figure 5. For the *h*S2VP/[*h*Im][TFSI] mixtures, the $T_{g,PS}$ is in the vicinity of 100 °C because of the near-complete partitioning of [Im][TFSI] in the P2VP-rich microphase. In contrast, mixtures containing [*d*Im][TFSI] exhibit a lower $T_{g,PS}$. This finding is consistent with the SANS data that reveal a significant concentration of [*d*Im][TFSI] in the PS-rich microphase.

Our DSC measurements on [*h*Im][TFSI] and [*d*Im][TFSI] indicate that the melting temperature of the salts were within experimental error (72−74 °C), but the heat of fusion of [*h*Im][TFSI] ($\Delta H_{fus} = 18.2 \pm 2.8$ kJ/mol) was slightly less than that of [*d*Im][TFSI] ($\Delta H_{fus} = 21.1 \pm 1.4$ kJ/mol). Simple theories based on ideal solution thermodynamics would indicate that [*h*Im][TFSI] would be expected to exhibit higher solubility in a nonpolar polymer such as PS. The fact that we observe the opposite effect indicates the need for more sophisticated theories for understanding the interplay between molecular structure and solubility of ionic liquids in polymers.

On the basis of χ measurements of hydrogenated versus deuterated polymers, such as PS and poly(methyl methacrylate),[31] we anticipate variations on the order of 0.001 for $\chi_{PS/P2VP}$ caused by deuterium labeling. It is thus not surprising that deuteration of the copolymers has little effect on thermodynamics. Much less is known about the effect of deuteration on ionic interactions and hydrogen bonding. These effects are likely to play an important role in determining ionic liquid partitioning of S2VP/[Im][TFSI] mixtures. Tsuda et al. have demonstrated a monotonic increase in the strength of hydrogen bonding interactions with ϕ_P in mixtures of a poly(ethylene oxide)-based homopolymer and 1-ethyl-3-methylimidazolium [TFSI] mixtures related to the properties of disassociated ions and their interactions with polymer chains.[32] Similar effects might underlie our observations in S2VP/[Im][TFSI] mixtures.

Conclusions

We have examined the distribution of an [Im][TFSI] ionic liquid within microphase-separated S2VP copolymer domains in concentrated mixtures of the two components. Using SANS contrast matching and DSC, we established that the ionic liquid selectively partitions into P2VP domains for mixtures in the composition range $0.51 \leq \phi_P \leq 0.86$. Much more precise measurements of the distribution of ionic liquid would be possible if the extent of intermixing of the PS and P2VP blocks in the presence of ionic liquid was known from independent experiments. Despite this limitation, we show conclusively that deuterated [Im][TFSI] is present in both PS-rich and P2VP-rich microphases, whereas hydrogenated [Im][TFSI] is mainly present in the P2VP-rich microphase. Further work is needed to determine the underpinnings of this unexpected deuterium labeling effect.

Acknowledgment. We gratefully acknowledge support from the Assistant Secretary for Energy Efficiency and Renewable Energy, Office of Hydrogen, Fuel Cell, and Infrastructure Technologies of the U.S. Department of Energy under contract no. DE-AC02-05CH11231. We acknowledge the support of the NIST, U.S. Department of Commerce, in providing the neutron research facilities used in this work. The initial neutron scattering experiments were conducted at Oak Ridge National Laboratory's (ORNL) High Flux Isotope Reactor, which is sponsored by the Scientific User Facilities Division, Office of Basic Energy Sciences, U.S. Department of Energy. We gratefully acknowledge Dr. Andrew Jackson for experimental assistance at NIST and Dr. Yuri Melnichenko and Dr. Gang Cheng for experimental assistance at ORNL.

Supporting Information Available: Definition of variables, SANS profiles, ionic liquid distribution model intensity fits and associated compositions, and temperature dependence of PS/P2VP mixing. This material is available free of charge via the Internet at http://pubs.acs.org.

References and Notes

(1) Bates, F. S.; Fredrickson, G. H. *Phys. Today* **1999**, *52*, 32–38.
(2) Ueki, T.; Watanabe, M. *Macromolecules* **2008**, *41*, 3739–3749.
(3) Wassercheid, P.; Welton, T. *Ionic Liquids in Synthesis*; Wiley-VCH: Weinheim, Germany, 2003.
(4) Fuller, J.; Breda, A. C.; Carlin, R. T. *J. Electrochem. Soc.* **1997**, *144*, L67–L70.
(5) Doyle, M.; Choi, S. K.; Proulx, G. *J. Electrochem. Soc.* **2000**, *147*, 34–37.
(6) Lee, J.; Kaake, L. G.; Cho, J. H.; Zhu, X. Y.; Lodge, T. P.; Frisbie, C. D. *J. Phys. Chem. C* **2009**, *113*, 8972–8981.
(7) Soo, P. P.; Huang, B. Y.; Jang, Y. I.; Chiang, Y. M.; Sadoway, D. R.; Mayes, A. M. *J. Electrochem. Soc.* **1999**, *146*, 32–37.
(8) Singh, M.; Odusanya, O.; Wilmes, G. M.; Eitouni, H. B.; Gomez, E. D.; Patel, A. J.; Chen, V. L.; Park, M. J.; Fragouli, P.; Iatrou, H.; Hadjichristidis, N.; Cookson, D.; Balsara, N. P. *Macromolecules* **2007**, *40*, 4578–4585.
(9) He, Y. Y.; Li, Z. B.; Simone, P.; Lodge, T. P. *J. Am. Chem. Soc.* **2006**, *128*, 2745–2750.
(10) Simone, P. M.; Lodge, T. P. *Macromolecules* **2008**, *41*, 1753–1759.
(11) Virgili, J. M.; Hexemer, A.; Pople, J. A.; Balsara, N. P.; Segalman, R. A. *Macromolecules* **2009**, *42*, 4604–4613.
(12) Lodge, T. P.; Hamersky, M. W.; Hanley, K. J.; Huang, C. I. *Macromolecules* **1997**, *30*, 6139–6149.
(13) Virgili, J. M.; Tao, Y. F.; Kortright, J. B.; Balsara, N. P.; Segalman, R. A. *Macromolecules* **2007**, *40*, 2092–2099.
(14) Gomez, E. D.; Panday, A.; Feng, E. H.; Chen, V.; Stone, G. M.; Minor, A. M.; Kisielowski, C.; Downing, K. H.; Borodin, O.; Smith, G. D.; Balsara, N. P. *Nano Lett.* **2009**, *9*, 1212–1216.
(15) Yokoyama, H.; Mates, T. E.; Kramer, E. J. *Macromolecules* **2000**, *33*, 1888–1898.
(16) Noda, A.; Susan, A. B.; Kudo, K.; Mitsushima, S.; Hayamizu, K.; Watanabe, M. *J. Phys. Chem. B* **2003**, *107*, 4024–4033.
(17) Yang, H.; Shibayama, M.; Stein, R. S.; Shimizu, N.; Hashimoto, T. *Macromolecules* **1986**, *19*, 1667–1674.
(18) Rudd, J. F. Physical Constants of Polystyrene. In *Polymer Handbook*, 3rd ed.; Brandrup, J., Immergut, E. H., Eds.; John Wiley and Sons: New York, 1989; p 82.
(19) Glinka, C. J.; Barker, J. G.; Hammouda, B.; Krueger, S.; Moyer, J. J.; Orts, W. J. *J. Appl. Crystallogr.* **1998**, *31*, 430–445.
(20) Kline, S. R. *J. Appl. Crystallogr.* **2006**, *39*, 895–900.
(21) Higgins, J. S.; Benoit, H. C. *Polymers and Neutron Scattering*; Clarendon Press: Oxford, U.K., 1994.
(22) Strazielle, C.; Benoit, H. *Macromolecules* **1975**, *8*, 203–205.
(23) Bates, F. S.; Wignall, G. D.; Koehler, W. C. *Phys. Rev. Lett.* **1985**, *55*, 2425–2428.
(24) Buckingham, A. D.; Hentschel, H. G. E. *J. Polym. Sci., Part B: Polym. Phys.* **1980**, *18*, 853–861.
(25) Graessley, W. W.; Krishnamoorti, R.; Balsara, N. P.; Fetters, L. J.; Lohse, D. J.; Schulz, D. N.; Sissano, J. A. *Macromolecules* **1993**, *26*, 1137–1143.
(26) Semenov, A. N. *Macromolecules* **1989**, *22*, 2849–2851.
(27) Helfand, E.; Tagami, Y. *J. Chem. Phys.* **1972**, *56*, 3592–3601.
(28) Shull, K. R. *Macromolecules* **1992**, *25*, 2122–2133.
(29) Huang, C. I.; Hsueh, H. Y. *Polymer* **2006**, *47*, 6843–6856.
(30) Dai, K. H.; Kramer, E. J. *Polymer* **1994**, *35*, 157–161.
(31) Balsara, N. P.; Eitouni, H. B. Thermodynamics of Polymer Blends. In *Physical Properties of Polymers*, 2nd ed.; Mark, J. E., Ed.; Springer: New York, 2006.
(32) Tsuda, R.; Kodama, K.; Ueki, T.; Kokubo, H.; Imabayashi, S.; Watanabe, M. *Chem. Commun.* **2008**, *40*, 4939–4941.